EVALUATION OF TWO CYCLIC-STRAIN IMPACT ATTENUATORS

RICHARD F. MANAGAN, CHIEF MASTER SERGEANT
KENNETH C. FLAGG, SECOND LIEUTENANT, USAF
JOHN H. DUDDY
NEVILLE P. CLARKE, MAJOR, USAF, VC

FOREWORD

This study was conducted under Project 6301, "Aerospace Systems Personnel Protection," Task 630102, "Personnel Protection in Aerospace Systems," by the Vibration and Impact Branch, Biodynamics and Bionics Division, Biomedical Laboratory, Aerospace Medical Research Laboratories, Wright-Patterson Air Force Base, Ohio 45433.

These tests were initiated in response to a request from Aerospace Research Associates, Incorporated, 2017 West Garvey Avenue, West Covina, California 91790, and the devices which were tested were supplied by them.

Mr. John H. Duddy of Lockheed Missiles and Space Company, NASA Program Human Factors, Department 55–60, P.O. Box 504, Sunnyvale, California 94088, worked on this evaluation during his reserve tour under a project training program.

The authors are particularly indebted to Mr. Daniels of Aerospace Research Associates, Incorporated, for his assistance in the conduct of the tests. Special acknowledgment is due Mr. Harold Wooding, Mr. Theodore Ring, and Mr. Ivan Jankowski for the operation of the Vertical Decelerator and the electronic data gathering systems. The tests were conducted during February and March 1965.

This technical report has been reviewed and is approved.

J. W. HEIM, PhD
Technical Director
Biomedical Laboratory
Aerospace Medical Research Laboratories

ABSTRACT

Two impact energy attenuators operating on the principle of cyclic straining of materials were tested to determine: (1) maximum output accelerations and (2) resultant attenuator deflections. The attenuators were tested in tension with initial impact velocities from 914 to 1338 centimeters per second and maximum input accelerations from 21 G to 58 G. The attenuators were tested in compression with initial impact velocities from 546 to 855 centimeters per second. The maximum output acceleration showed dependency upon payload that was consistent with the attenuator design theory.

SECTION I
INTRODUCTION

As a part of its continuing effort to identify new energy absorbing materials and devices suitable for dissipating the landing impact energy of escape systems and manned space vehicles, the Vibration and Impact Branch has conducted a preliminary evaluation of two attenuators operating on the principle of cyclic straining of materials. These attenuators were designed by Aerospace Research Associates, Inc. The evaluation determined certain characteristics under dynamic loads representative of the envelope of spacecraft landing impact accelerations.

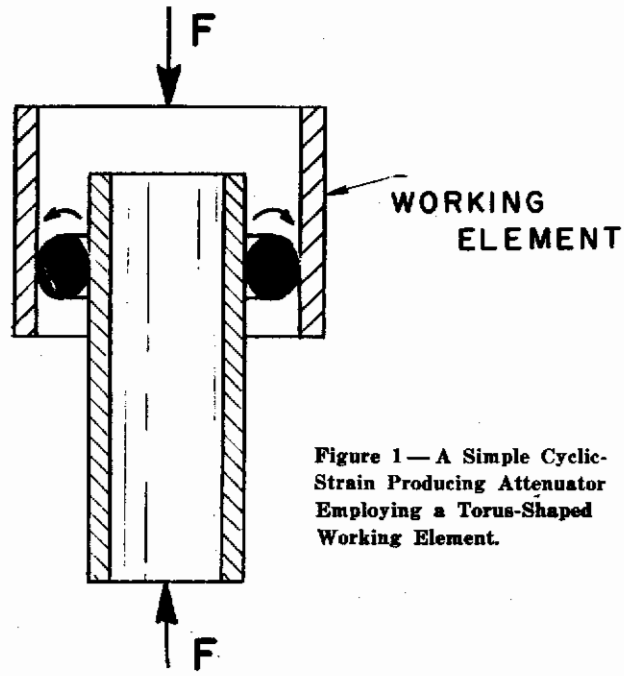

Figure 1 — A Simple Cyclic-Strain Producing Attenuator Employing a Torus-Shaped Working Element.

SECTION II
PRINCIPLE OF CYCLIC STRAIN ATTENUATION

A cyclic strain attenuator absorbs energy by converting unidirectional motion into cyclic deformation of material. Attenuators designed to produce cyclic strain require a force transmitting structure and deformable working elements. A working element may be a solid or tubular torus, or section of a torus. As the element is rolled around its neutral axis, cyclic tensile and compressive strain is produced in the longitudinal fibers of the material. A simple cyclic-strain producing attenuator employing a torus-shaped working element is shown in figure 1. It may be repeatedly cycled in tension and compression up to the limit of its mechanical endurance. Performance is related to the cyclic stress-strain and fatigue of the material used for the working element or elements. Absorption per stroke depends upon the configuration of the hysteresis loops during cycling, which vary as a function of the material, change in the rate of the applied force, working hardening or softening of the material, friction within the device, number of working elements, and other factors. For the attenuator shown, energy absorbed per cycle generally varies directly as a function of the strain range through which the working element is cycled. Fatigue life generally varies inversely with the square of the strain range per cycle. *

SECTION III
TEST PROGRAM

PROGRAM OBJECTIVES

Two ARA attenuators were evaluated in terms of their usefulness as a means of reducing the mechanical force environment delivered to man carrying systems. The range of velocities and accelerations in which the attenuators were tested are representative of those encountered during ground landing of vehicles descending by parachute. The tests were designed to evaluate the performance of the attenuators as a function of: (a) peak input acceleration, (b) impact velocity, (c) mass of payload, and (d) direction of force, i.e., compression or tension loads applied to the attenuators. They were designed to provide the same peak output acceleration for a given payload regardless of input acceleration (provided sufficient dynamic load is provided to initiate stroking) and impact velocity. The peak output acceleration is supposed to be a predictable function of the payload mass. They were also designed to perform the same whether the applied force is in tension or compression. The ancillary objectives of the program were: (a) determination of static tensile and compressive loads required to initiate and sustain displacement of working elements and (b) comparison of yield force between static and dynamic application of load.

* Platus, D. L., et. al., Interim Final Report on Concepts of Multiple-Impact Study of Energy Absorption, ARA Report No. 89, Aerospace Research Associates, Inc., 2017 W Garvey Ave, West Covina, Calif 91790, 15 May 1964.

DESCRIPTION OF TEST ARTICLES *

The two prototype cyclic-strain energy absorption devices were identified as ARA attenuator numbers 100 and 101. They consisted of two concentric stainless steel tubes with torus elements held captive in the space between the tubes as illustrated in fig. 2. The torus elements were AISI type-304, stainless-steel rings with a circular cross section and with unjoined ends. The torus elements were driven by friction coupling between the ring and the cylindrical tubes produced by built-in dimensional interference. The diameter of the wire used to fabricate the rings was slightly larger than the space between the cylindrical tubes. As the concentric tubes were displaced with respect to one another by withdrawing or inserting the inner tube, each torus element was rolled longitudinally, producing cyclic tensile and compressive straining of longitudinal fibers except at the neutral axis of the wire. Table I summarizes the principle design features of the attenuators.

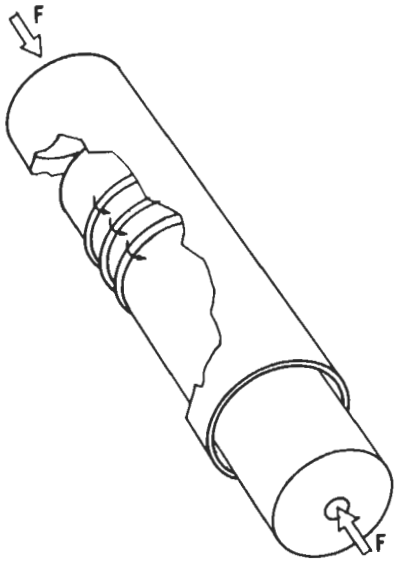

Figure 2 — An ARA Attenuator.

TABLE I

ATTENUATOR DESIGN FEATURES

Attenuator	Design Yield Force dynes	Number of Torus Elements	Maximum Stroke centimeters
100	1.134×10^9	12	27.94
101	1.222×10^9	13	27.68

*All numbers in this report have units consistent with the metric absolute (or cgs) system.

APPROACH

The program consisted of 9 tests to validate the procedure, 15 dynamic tension tests, 9 dynamic compression tests, and intervening static tests to determine any change in static characteristics after dynamic loading. Table II gives the conditions of each test of the program.

DYNAMIC TENSION TESTS

The AMRL Vertical Deceleration Tower, illustrated in fig. 3, was used to perform the dynamic tension tests. The Verical Deceleration Tower consists of a carriage mounted on a pair of 1524-cm vertical tracks. Test articles are attached to the carriage, which is raised by a hoist and released for free fall. The carriage deceleration mechanism consists of a tapered plunger, an integral part of the carriage, which falls into a water filled cylinder. The deceleration profile may be varied by changing (1) the distance of free fall, (2) the plunger taper, or (3) the orifice diameter of the water filled cylinder. The attenuators were attached to the Vertical Deceleration Tower carriage with a ball-joint fitting as shown in fig. 4. The payload masses were attached to the bottom of the attenuators. Input accelerations were measured by an accelerometer attached to the top face of the attenuators and output accelerations were measured by an accelerometer attached to the top of the payload mass.

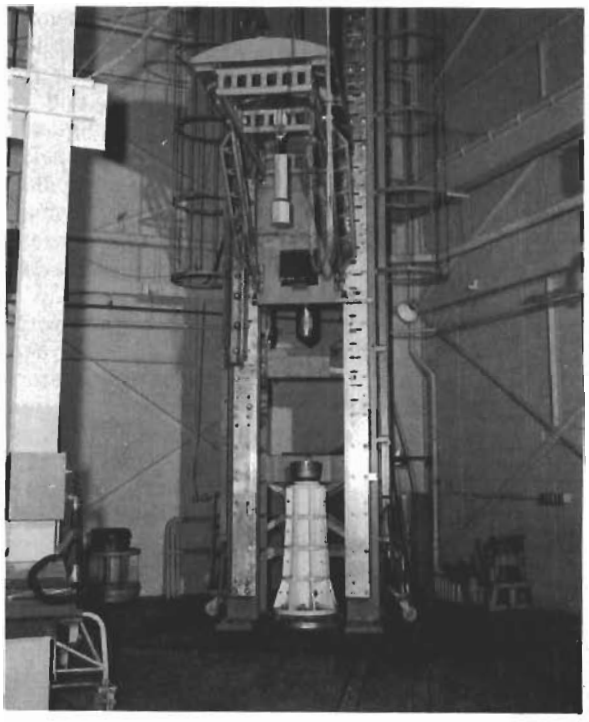

Figure 3 — AMRL Vertical Deceleration Tower.

TABLE II. CONDITIONS FOR EACH TEST

TEST	ENVIRONMENT	ATTENUATOR	DROP HEIGHT cm	PAYLOAD MASS grams	REMARKS
1–7	PROCEDURE VALIDATION FOR DYNAMIC TENSION TESTS				
8	DYNAMIC TENSION	101	426.7	7.716x10 ^{4}	
9	"	101	548.6	7.716x10 ^{4}	
10	"	100	426.7	7.716x10 ^{4}	
11	"	100	548.6	7.716x10 ^{4}	
12	"	100	914.4	7.716x10 ^{4}	
13	"	100	914.4	4.085x10 ^{4}	
14	"	100	914.4	5.901x10 ^{4}	S.C.
15	"	101	914.4	4.085x10 ^{4}	
16	"	101	914.4	5.901x10 ^{4}	S.C.
17–18	PROCEDURE VALIDATION FOR DYNAMIC COMPRESSION TESTS				
19	DYNAMIC COMPRESSION	101	167.6	10.667x10 ^{4}	S.T.
20	"	100	152.4	10.667x10 ^{4}	S.T.
21	"	101	167.6	7.399x10 ^{4}	
22	"	101	208.3	7.399x10 ^{4}	S.T.
23	"	100	152.4	7.399x10 ^{4}	
24	"	100	190.5	7.399x10 ^{4}	S.T.
25	"	101	279.4	7.399x10 ^{4}	S.T.
26	"	100	342.9	7.399x10 ^{4}	S.T.
27	"	101	373.4	7.399x10 ^{4}	S.T.
28	DYNAMIC TENSION	100	426.7	7.716x10 ^{4}	
29	"	100	548.6	7.716x10 ^{4}	S.C.
30	"	101	426.7	7.716x10 ^{4}	
31	"	101	548.6	7.716x10 ^{4}	S.C.
32	"	101	426.7	7.716x10 ^{4}	S.C.
33	"	100	426.7	7.716x10 ^{4}	S.C.

ST = TEST FOLLOWED BY A STATIC TENSION TEST.
SC = TEST FOLLOWED BY A STATIC COMPRESSION TEST.

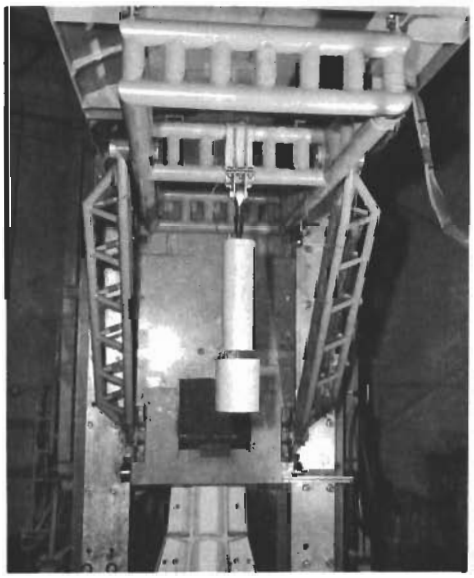

Figure 4 — Mounting of Attenuator to Carriage of the Deceleration Tower.

DYNAMIC COMPRESSION TESTS

The Barry Varipulse Shock Machine (Model 15575–2) was used to perform the dynamic compression tests. The Varipulse Shock Machine consists of a carriage mounted on a pair of vertical tracks. Test articles are attached to the carriage, which is raised and released for free fall. The carriage is decelerated by impact with an anvil. The magnitude of the deceleration profile may be varied by changing the distance of free fall. The attenuators were attached to the Varipulse Shock Machine carriage shown in fig. 5. Output accelerations were measured by an accelerometer located at the geometic center of the top face of the carriage.

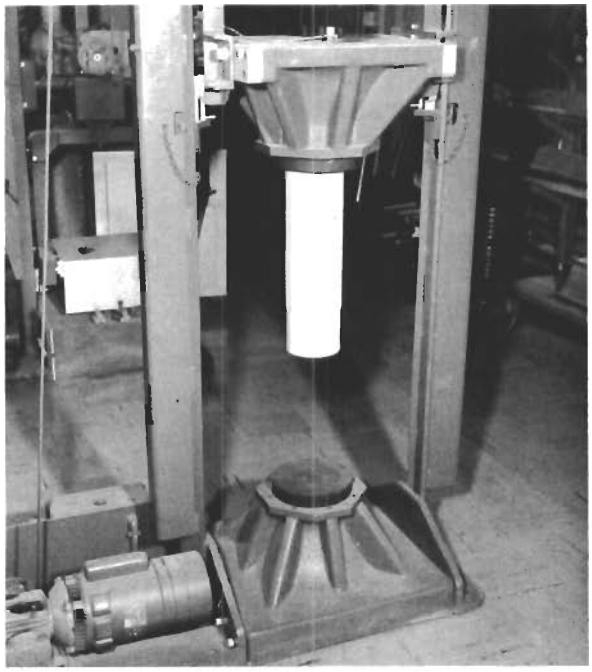

Figure 5 — Mounting of Attenuator to Varipulse Shock Machine.

STATIC TESTS

The Baldwin Testing Machine (Model SO 49860) was used to perform the static dynamic and compression tests. As each attenuator was dynamically cycled to the limits of its stroke, it was removed from the dynamic facility, mounted in the Baldwin Testing Machine and recycled to restore it to the configuration required for the next dynamic test.

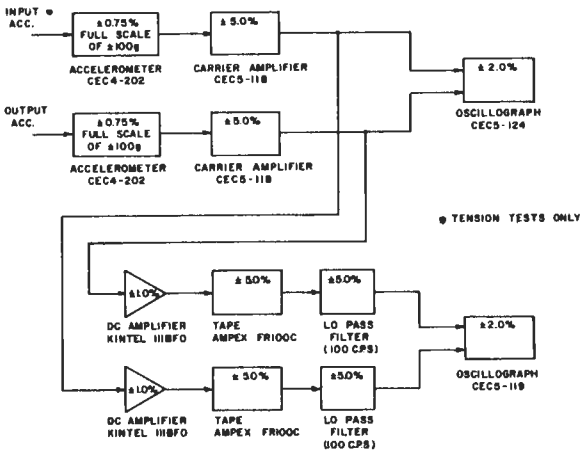

Figure 6 — Block Diagram of Dynamic Test Instrumentation.

INSTRUMENTATION

The instrumentation used for the dynamic tests is illustrated by the block shown in fig. 6. An Ampex FR100C tape recorder simultaneously recorded the accelerometer outputs to facilitate subsequently filtering of the data. The error estimations of the oscillograph traces are the square root of the sum of the squares of the accuracy values for each component. The estimations are shown in fig. 7.

Forces generated to initiate displacement of the attenuators during the static tests were recorded from the dial of the Baldwin Testing Machine. Average force to sustain displacement was also recorded.

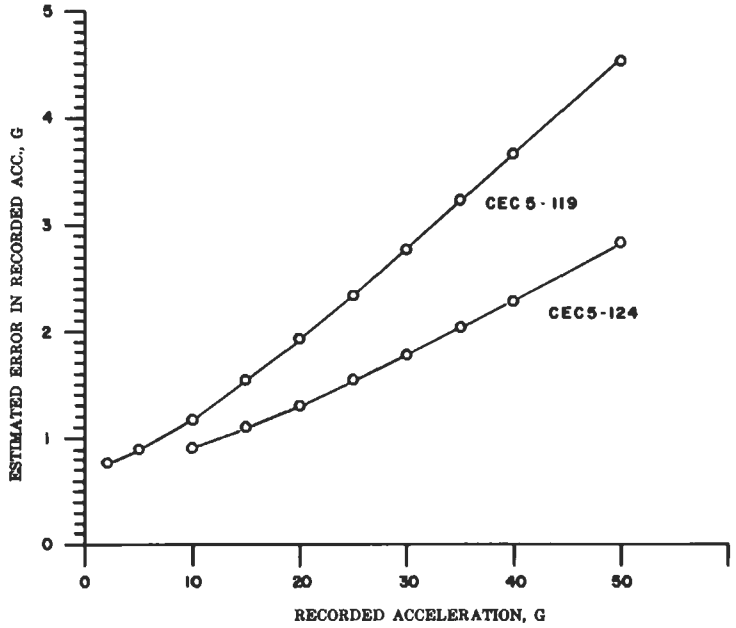

Figure 7 — Estimated Error in the Recorded Acceleration for the Dynamic Tests.

SECTION IV
TEST RESULTS

DYNAMIC TENSION TEST RESULTS FOR ATTENUATOR 100

The recorded input acceleration and recorded output acceleration as obtained from the CEC 5–119 oscillograph for the dynamic tension tests of attenuator 100 are shown in fig. 8. The maximum values of these accelerations and the measured resultant attenuator extensions are given for each test in table III. The payload masses and the initial impact velocities as determined from the drop height are also tabulated.

The maximum output accelerations and the resultant attenuator extensions are shown in fig. 9 as a function of the maximum input acceleration and in fig. 10 as a function of the initial impact velocity. These relations are derived from tests using the 7.716 x 10^4 gram payload mass.

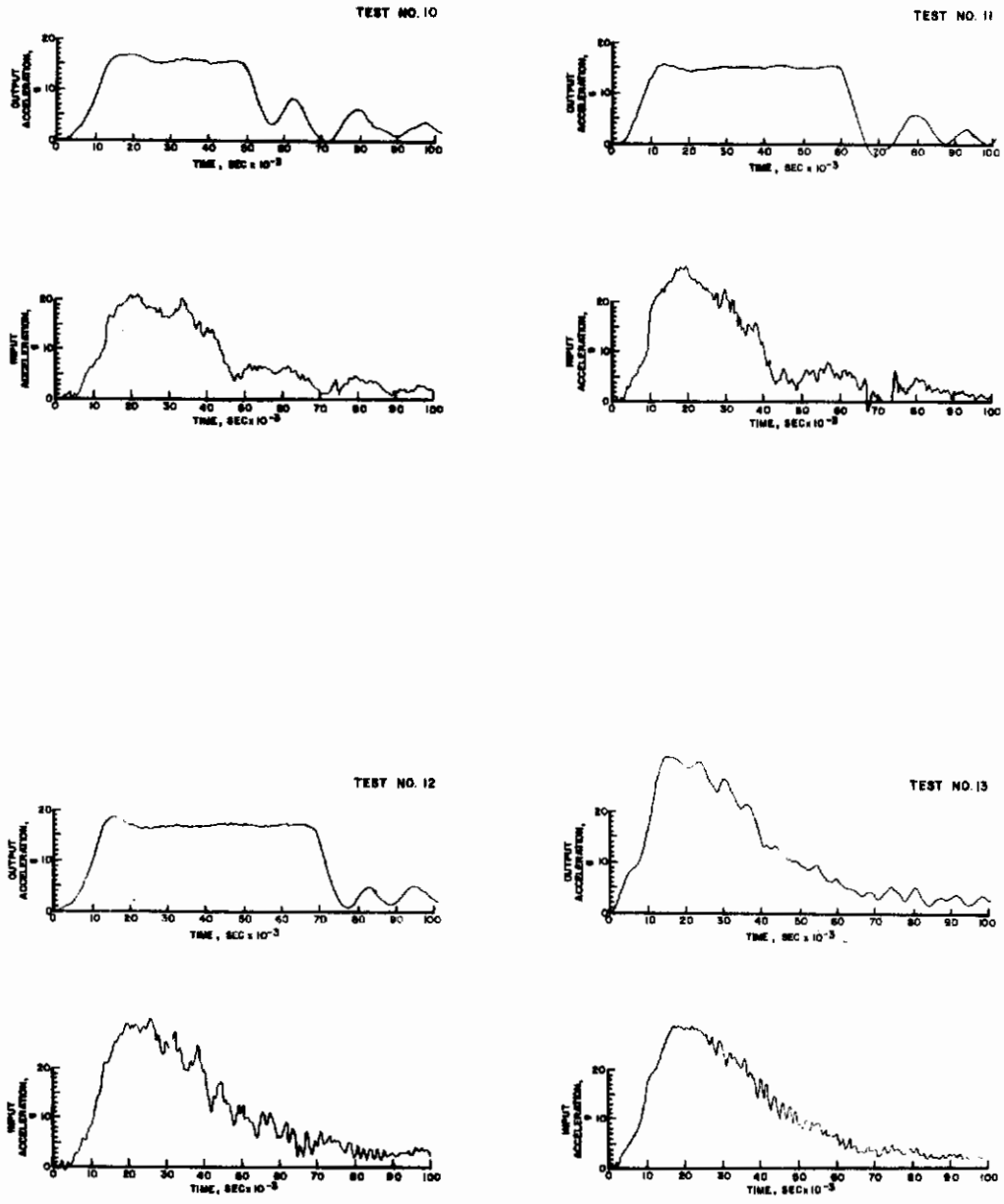

Figure 8 — Input and Output Acceleration Data from the Dynamic Tension Tests on Attenuator 100.

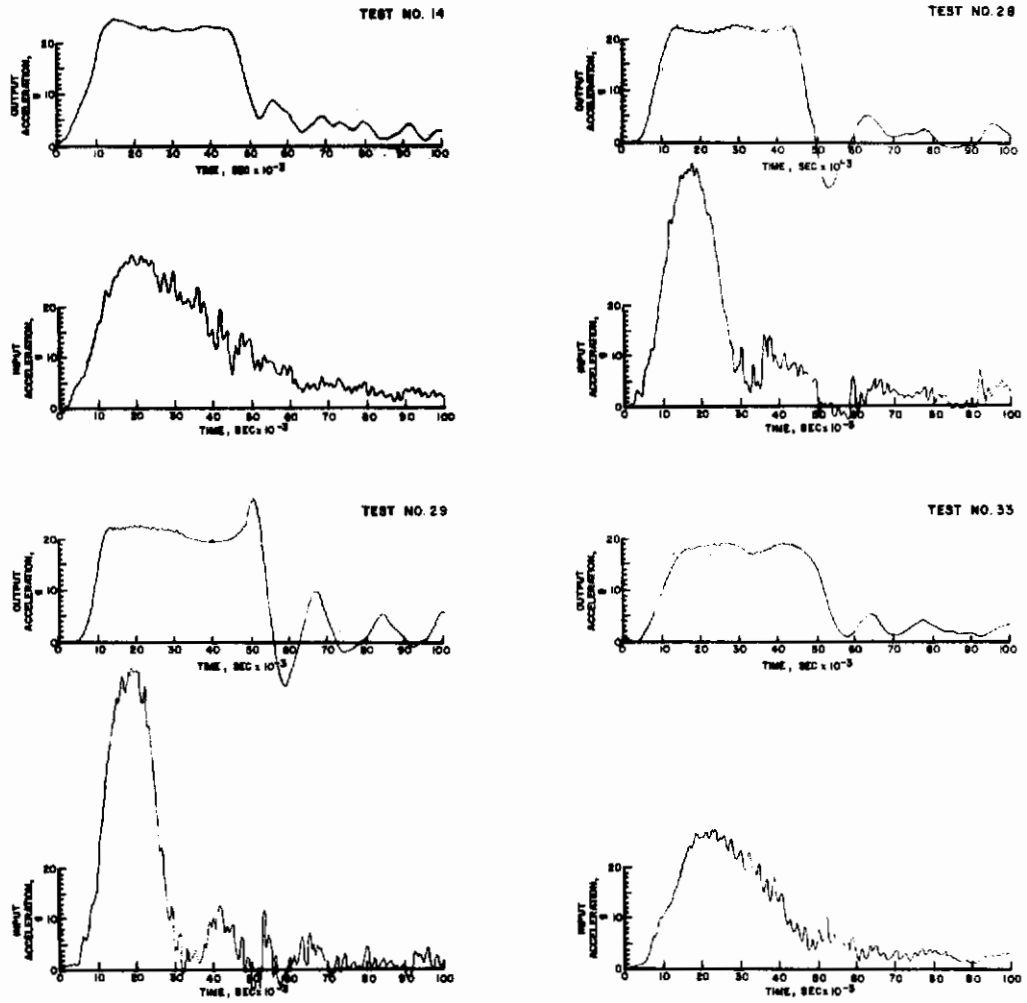

Figure 8 (Continued) — Input and Output Acceleration Data from the Dynamic Tension Tests on Attenuator 100.

TABLE III

DYNAMIC TENSION TEST RESULTS FOR ATTENUATOR 100

Test	Max Input Acceleration	Max Output Acceleration	Resultant Extension	Payload Mass	Initial Impact Velocity
	G	G	cm	grams	cm/sec
10	21.0	16.8	2.568	7.716×10^{4}	914
11	26.0	16.0	7.904	7.716×10^{4}	1037
12	28.4	18.3	10.957	7.716×10^{4}	1338
13	28.5	30.0	0.000	4.085×10^{4}	1338
14	28.5	24.5	2.667	5.901×10^{4}	1338
28 *	46.0	22.8	6.858	7.716×10^{4}	914
29	58.0	27.7	11.913	7.716×10^{4}	1037
33	25.8	18.5	4.505	7.716×10^{4}	914

* Before Test 28 the force required to statically recycle the attenuator increased above previously attained forces. After Test 28 an X-ray examination of the attenuator revealed a broken torus. Test 28 and later tests are not illustrated graphically.

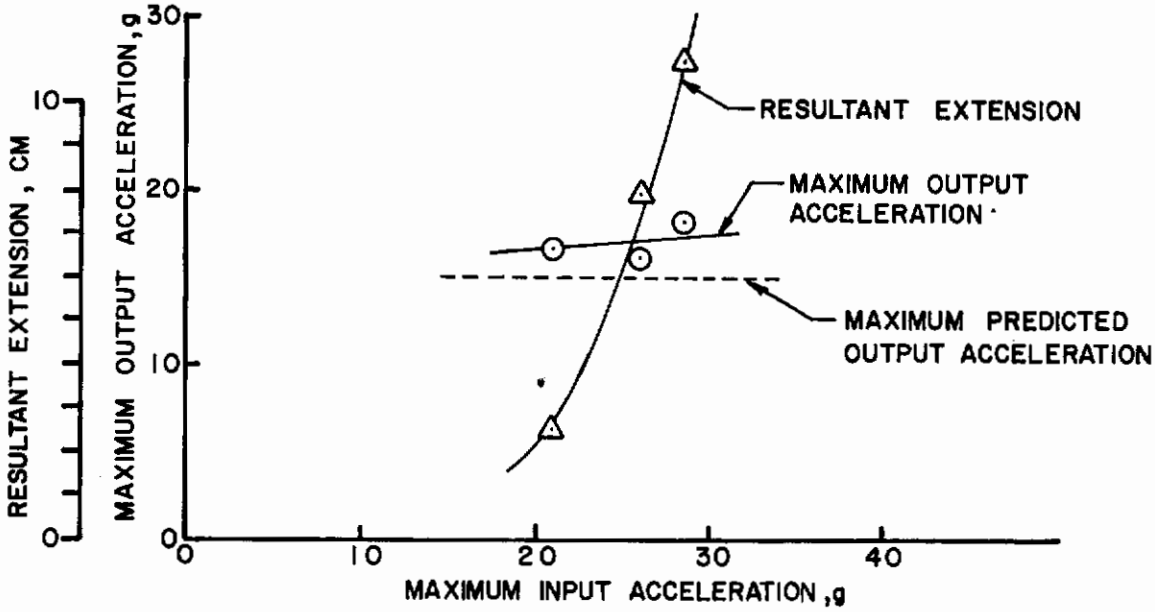

Figure 9 — Maximum Output Acceleration and Resultant Extension as a Function of Maximum Input Acceleration for the Dynamic Tension Tests on Attenuator 100.

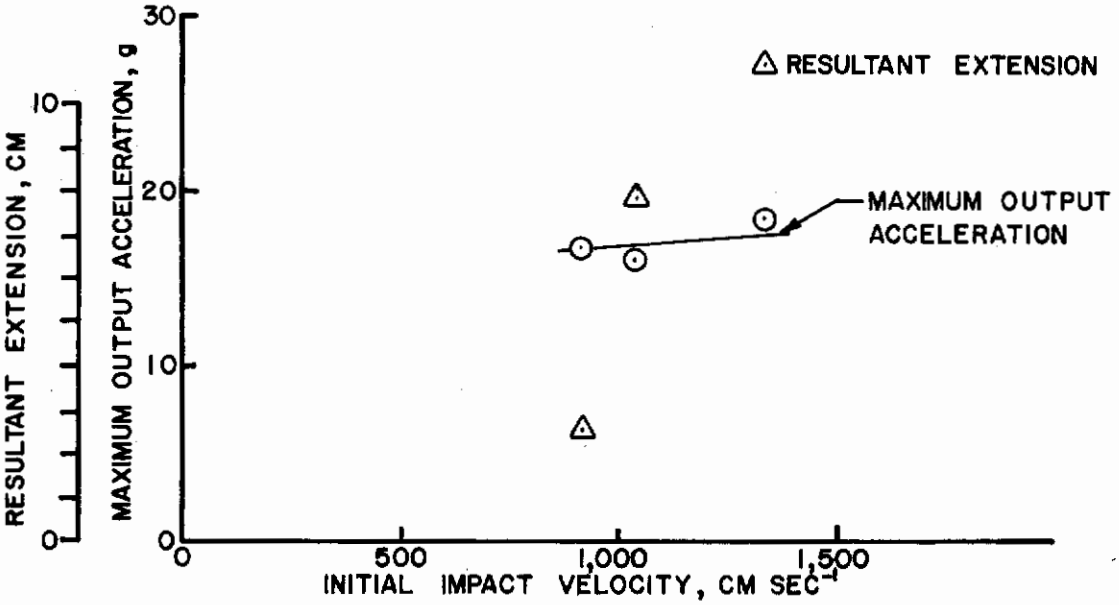

Figure 10 — Maximum Output Acceleration and Resultant Extension as a Function of Initial Impact Velocity for the Dynamic Tension Tests on Attenuator 100.

To illustrate the response as a function of mass, the ratio of the maximum experimental output acceleration to the maximum predicted output acceleration is shown in fig. 11 as a function of the payload mass. If the maximum input acceleration is less than the design yield force (see table I) divided by the payload mass, the maximum predicted output acceleration equals the maximum input acceleration. If the maximum input acceleration is greater than the design yield force divided by the payload mass, the maximum predicted output acceleration equals this quotient.

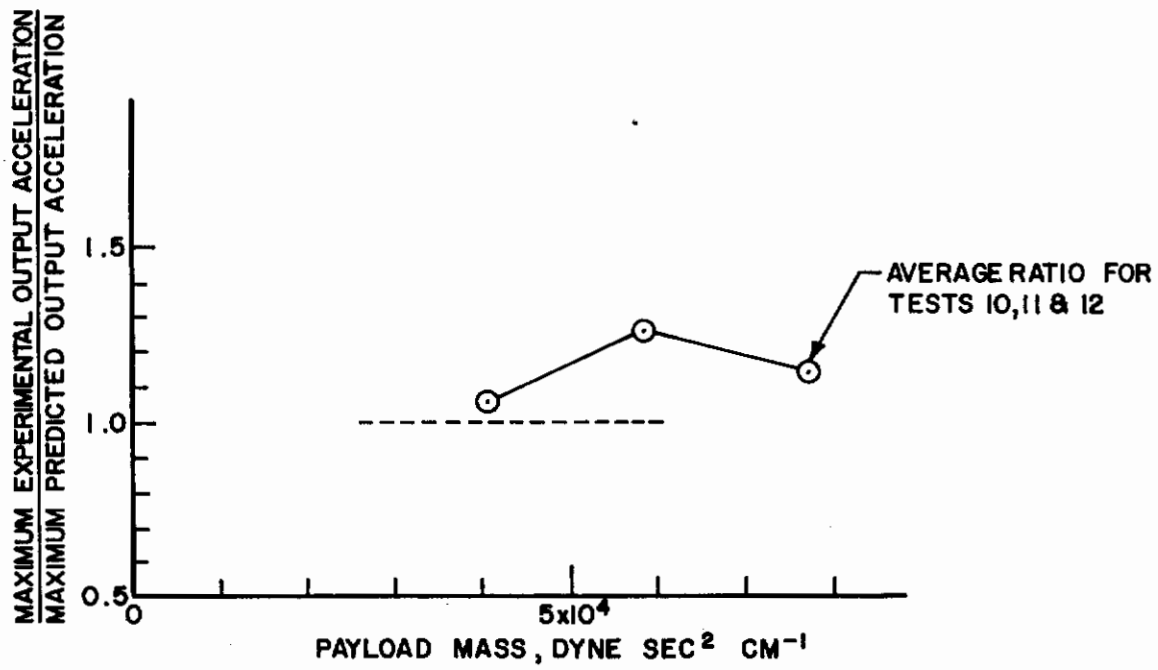

Figure 11 — Ratio of Maximum Experimental Output Acceleration to Maximum Predicted Output Acceleration as a Function of Payload Mass for the Dynamic Tension Tests on Attenuator 100.

DYNAMIC TENSION TEST RESULTS FOR ATTENUATOR 101

The recorded input and output acceleration as obtained from the CEC 5–119 oscillograph for the dynamic tension tests of attenuator 101 are shown in fig. 12. The maximum values of these accelerations and the measured resultant attenuator extensions are given for each test in table IV. The payload masses and the initial impact velocities are also tabulated as determined from the drop height.

TABLE IV

DYNAMIC TENSION TEST RESULTS FOR ATTENUATOR 101

Test	Max Input Acceleration	Max Output Acceleration	Resultant Extension	Payload Mass	Initial Impact Velocity
	G	G	cm	grams	cm/sec
9	30.2	20.1	4.417	7.716×10^4	1037
15	28.4	30.0	0.025	4.085×10^4	1338
16	29.1	21.4	6.223	5.901×10^4	1338
30	51.1	21.8	8.954	7.716×10^4	914
31	58.4	23.5	14.148	7.716×10^4	1037
32	26.5	19.2	3.353	7.716×10^4	914

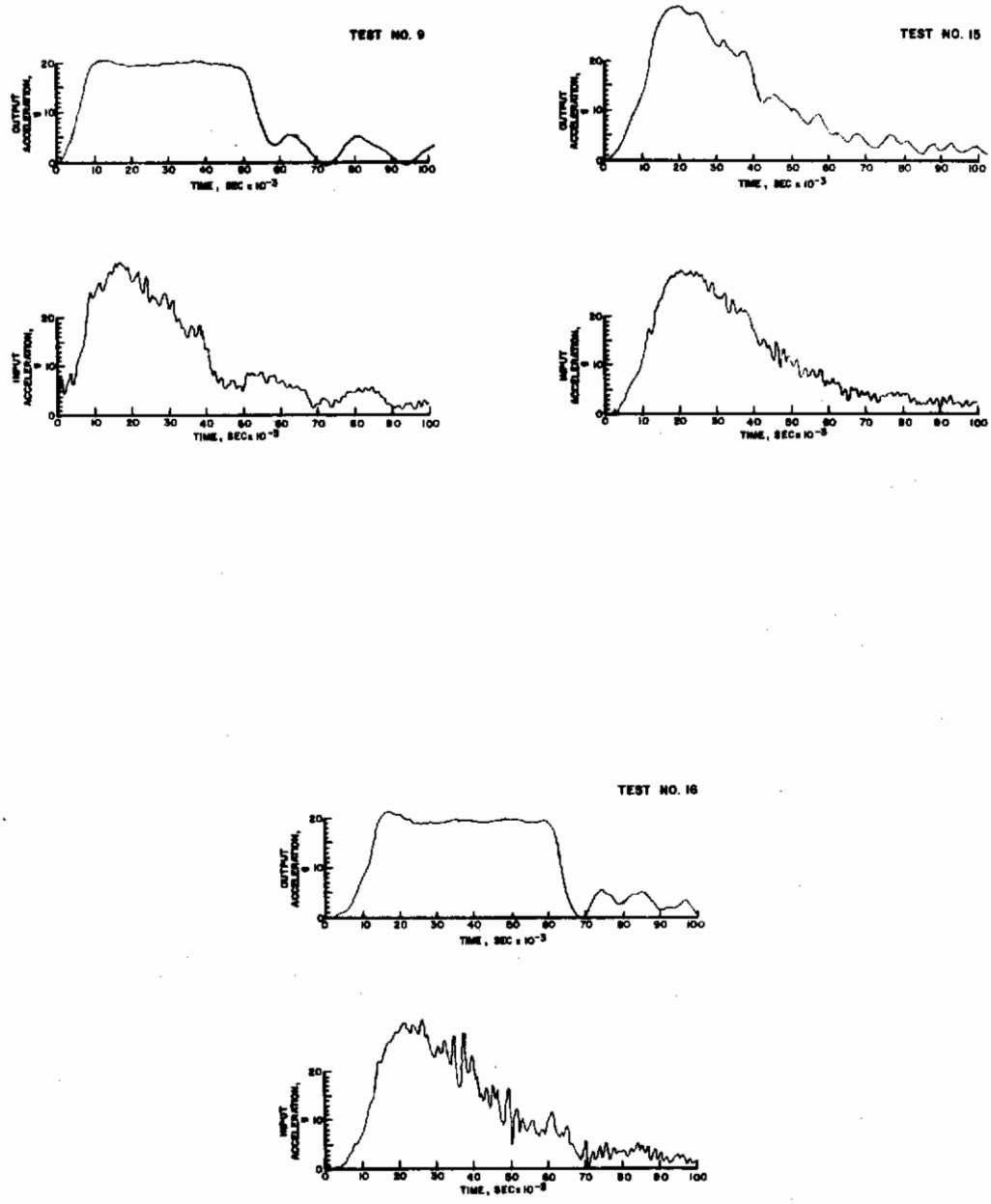

Figure 12 — Input and Output Acceleration Data from the Dynamic Tension Tests on Attenuator 101.

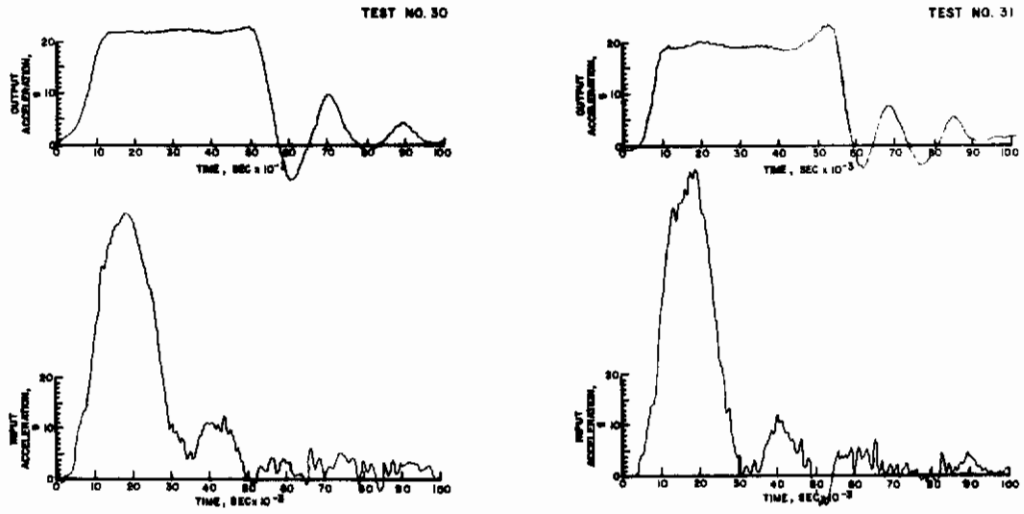

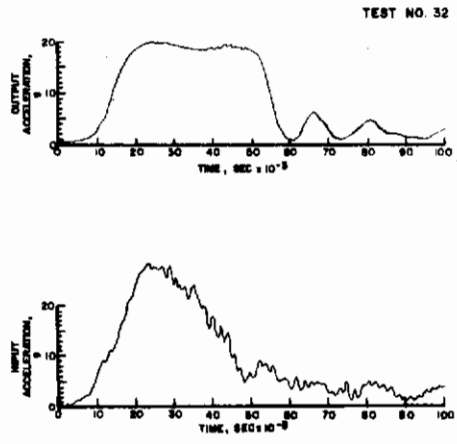

Figure 12 (continued) — Input and Output Acceleration Data from the Dynamic Tension Tests on Attenuator 101.

The maximum output accelerations and the resultant attenuator extensions are shown in fig. 13 as a function of the maximum input acceleration and in fig. 14 as a function of the initial impact velocity. These relations are derived from tests using only the 7.716×10^4 gram payload mass.

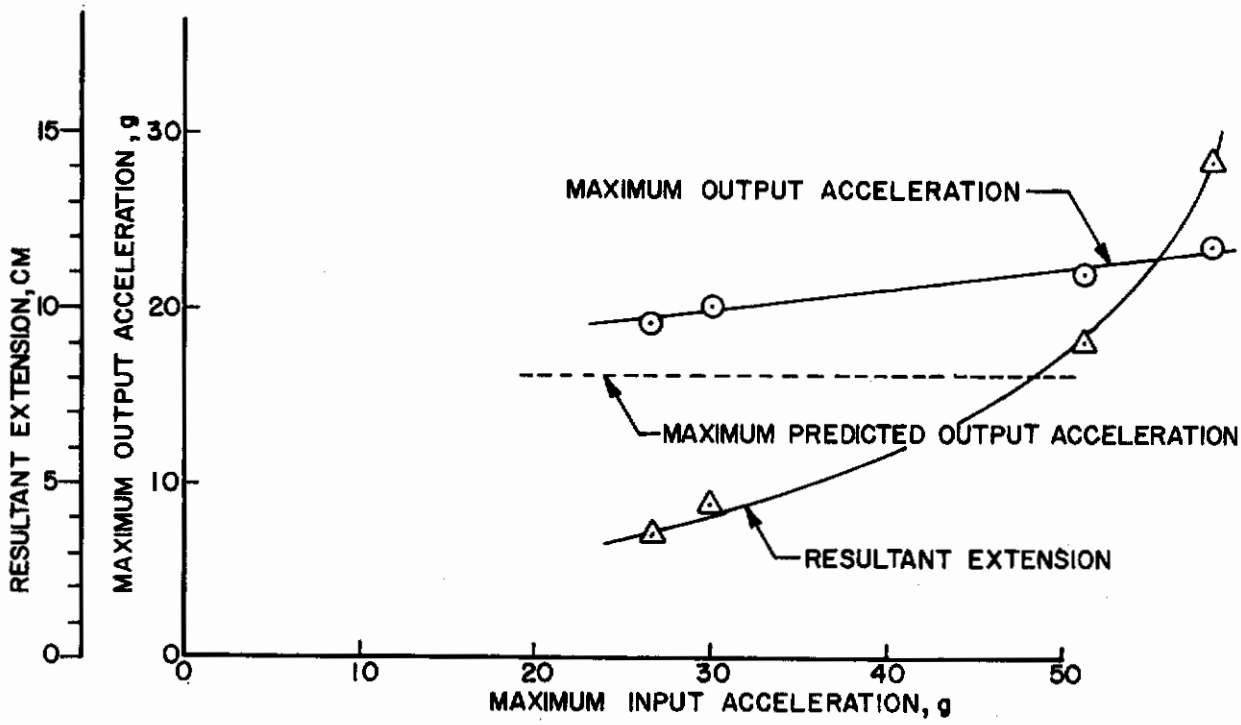

Figure 13 — Maximum Output Acceleration and Resultant Extension as a Function of Maximum Input Acceleration for the Dynamic Tension Tests on Attenuator 101.

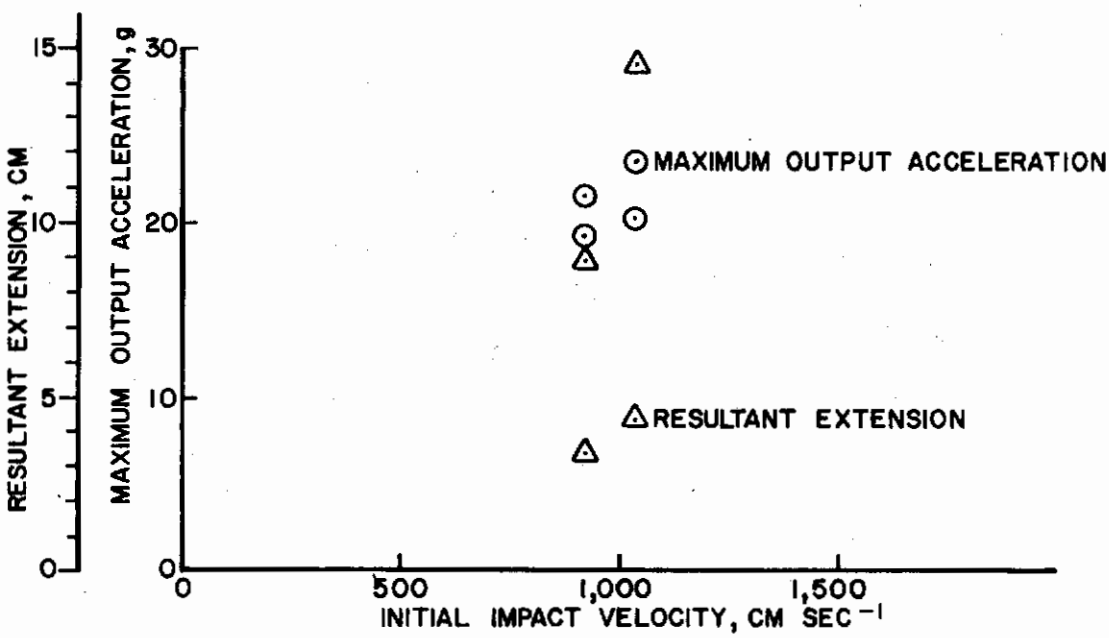

Figure 14 — Maximum Output Acceleration and Resultant Extension as a Function of Initial Impact Velocity for the Dynamic Tension Tests on Attenuator 101.

The ratio of the maximum experimental output acceleration to maximum predicted output acceleration is shown in fig. 15 as a function of the payload mass.

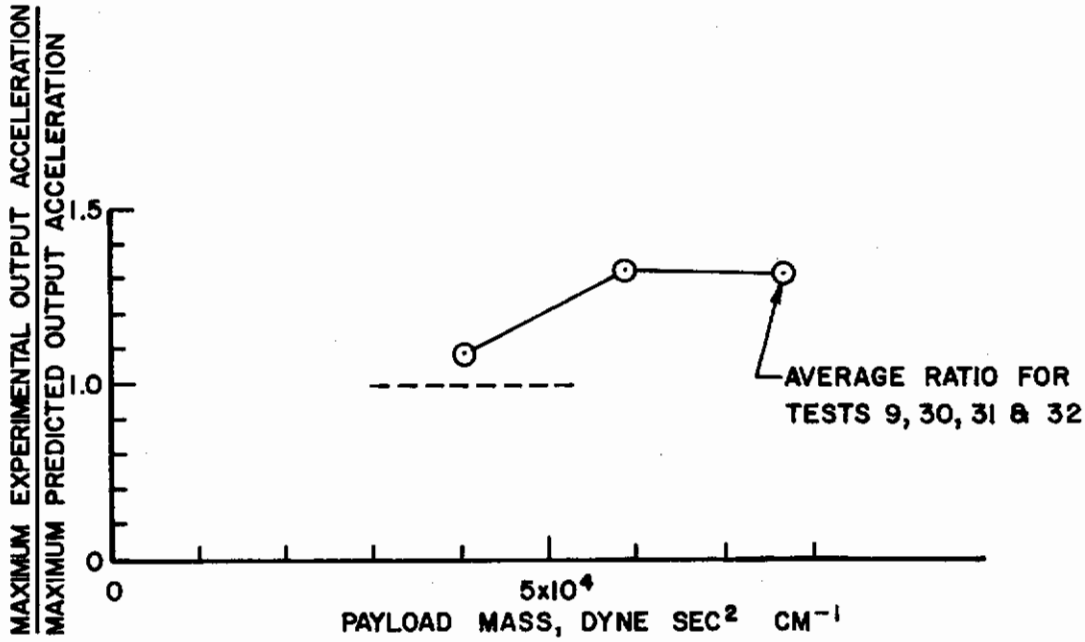

Figure 15 — Ratio of Maximum Experimental Output Acceleration to Maximum Predicted Output Acceleration as a Function of Payload Mass for the Dynamic Tension Tests on Attenuator 101.

DYNAMIC COMPRESSION TEST RESULTS FOR ATTENUATOR 100

The output acceleration data from the dynamic compression tests on Attenuator 100 are shown in fig. 16. The maximum values of these accelerations and the measured resultant attenuator compressions are given in table V. Also tabulated are the payload masses and the initial impact velocities as determined from the drop height.

The maximum output acceleration and resultant attenuator compressions are shown in fig. 17 as a function of initial impact velocity. These relations are derived from tests using only the 7.399 x 10^4 gram payload mass.

TABLE V

DYNAMIC COMPRESSION TEST RESULTS FOR ATTENUATOR 100

Test	Max Output	Compression	Payload Mass	Impact Velocity
	G	cm	grams	cm/sec
20	12.8	14.161	10.667 x 10^4	546.5
23	15.8	10.033	7.399 x 10^4	546.5
24	21.0	11.049	7.399 x 10^4	611.0
26	21.6	22.035	7.399 x 10^4	819.8

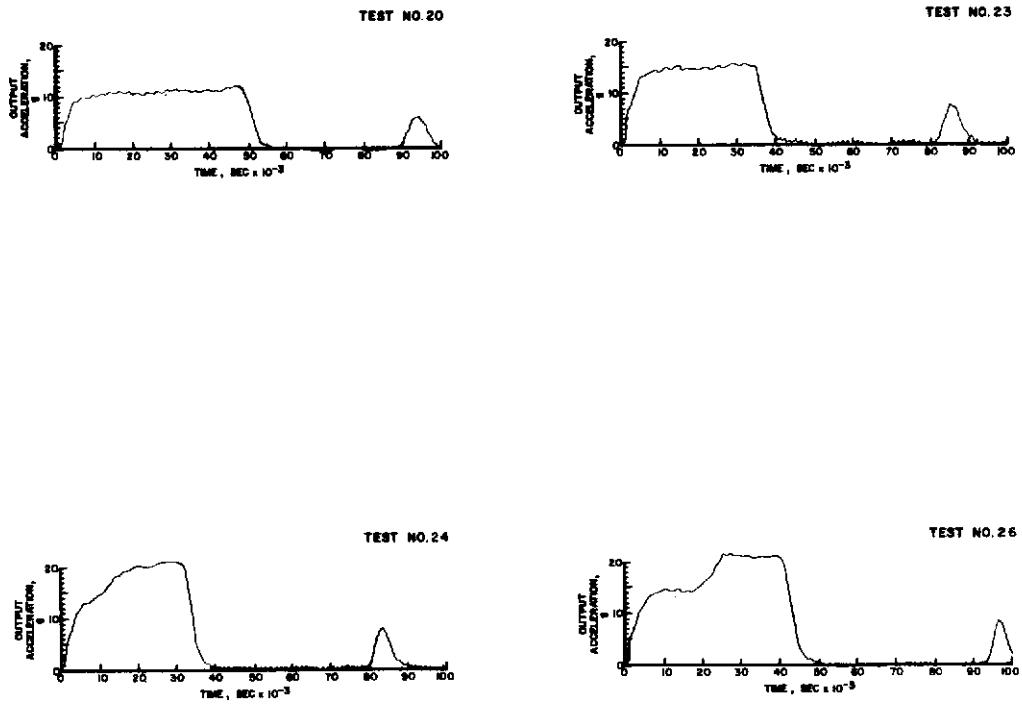

Figure 16 — Output Acceleration Data from the Dynamic Compression Tests on Attenuator 100.

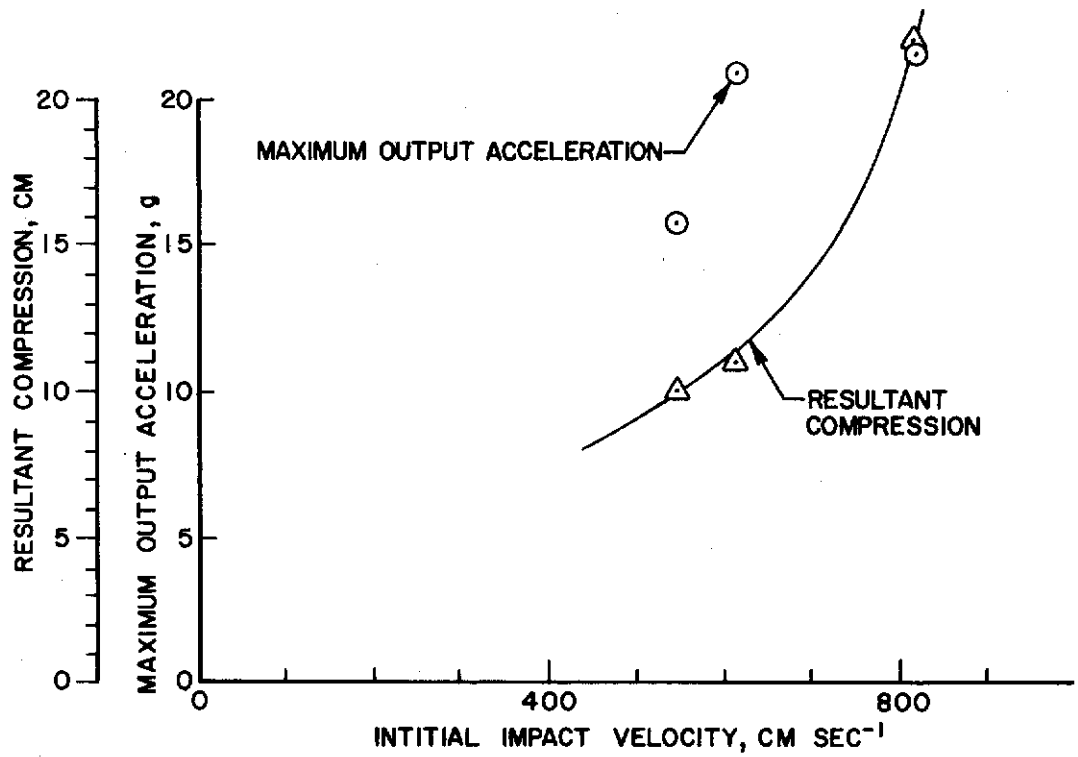

Figure 17 — Maximum Output Acceleration and Resultant Compression as a Function of Initial Impact Velocity for the Dynamic Compression Tests on Attenuator 100.

DYNAMIC COMPRESSION TEST RESULTS FOR ATTENUATOR 101

The output acceleration data from the dynamic compression tests on attenuator 101 are shown in fig. 18. The maximum values of these accelerations and the measured resultant attenuator compressions are given in table VI. Also tabulated are the payload masses and the initial impact velocities as determined from the drop height.

The maximum output acceleration and the resultant attenuator compressions are shown in fig. 19 as a function of initial impact velocity. These relations are derived from tests using the 7.399×10^{4} gram payload mass, only.

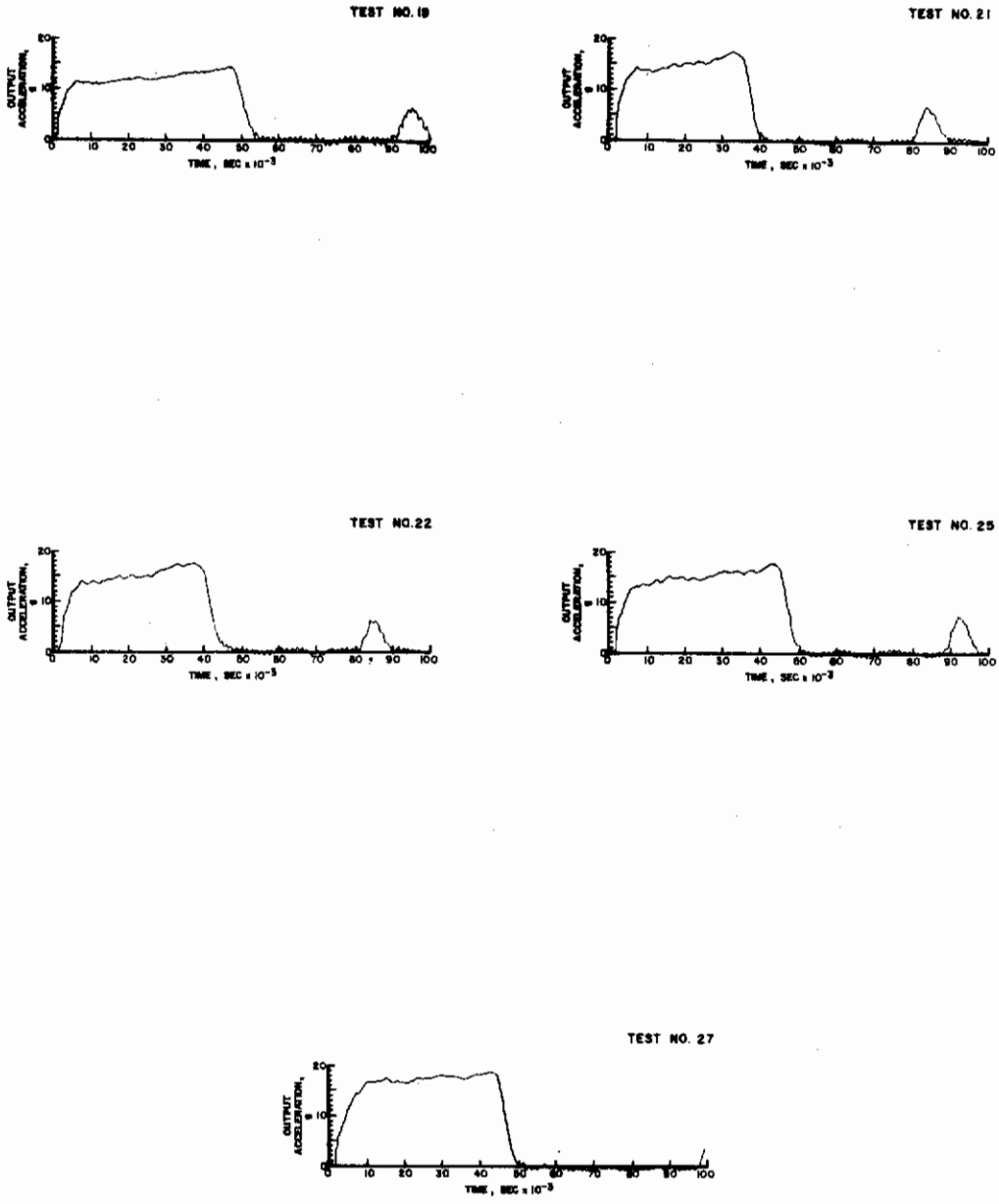

Figure 18 — Output Acceleration Data from the Dynamic Compression Tests on Attenuator 101.

TABLE VI

DYNAMIC COMPRESSION TEST RESULTS FOR ATTENUATOR 101

Test	Max Output Acceleration	Resultant Compression	Payload Mass	Initial Impact Velocity
	G	cm	grams	cm/sec
19	14.4	15.113	10.667×10^4	573.2
21	17.8	10.439	7.399×10^4	573.2
22	17.6	13.437	7.399×10^4	638.9
25	19.0	18.161	7.399×10^4	737.2
27	19.2	20.066	7.399×10^4	855.4

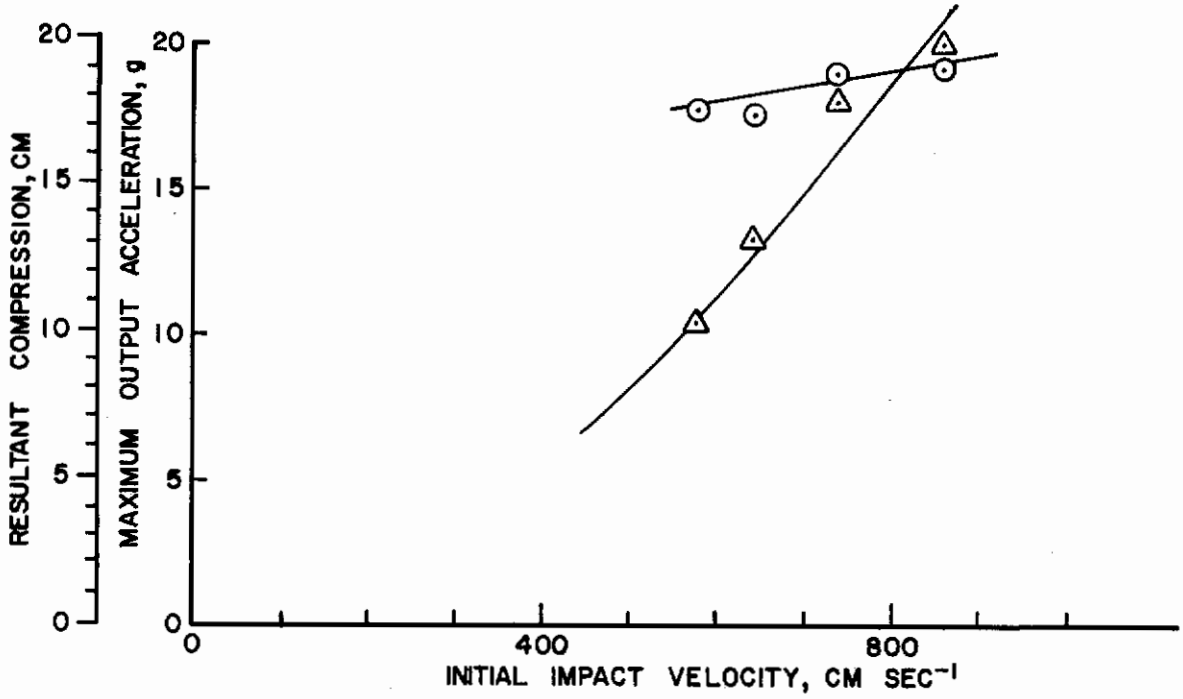

Figure 19 — Maximum Output Acceleration and Resultant Compression as a Function of Initial Impact Velocity for the Dynamic Compression Tests on Attenuator 101.

STATIC TEST RESULTS

The results of the static tests are tabulated in table VII. Averages for attenuator 100 exclude values obtained after dynamic test 26.

TABLE VII

STATIC TEST RESULTS

	Attenuator	Design Yield dynes	Measured Yield dynes	Average Force to Sustain dynes
Tension	100	1.089×10^9	1.201×10^9	1.134×10^9 dynes
Tension	101	1.223×10^9	1.303×10^9	1.223×10^9
Compression	100	1.089×10^9	0.756×10^9	1.134×10^9
Compression	101	1.223×10^9	1.303×10^9	1.223×10^9

SECTION IV

DISCUSSION

The maximum predicted output acceleration was the only base of comparison between designed dynamic responses and the measured dynamic responses of the two attenuators tested in this program. The graphic presentation of the data shows that the maximum predicted output acceleration can indeed approximate the maximum measured output acceleration. The decision as to whether this approximation is good enough must be made in consideration of the intended use.

There were no data collected in this program to quantitate the repeatibility of the dynamic responses of the attenuators. The importance of quantitating repeatibility must, also, be determined in consideration of the intended use.

During the course of testing, attenuator 100 was found to have developed a broken torus. Tests effected by this were not illustrated graphically but the data for these tests are given (see table III and fig. 8), and can be seen to give output accelerations that are inconsistent with the predicted values. There was no attempt made to relate this to a usable life for the attenuator.

Security Classification

DOCUMENT CONTROL DATA - R & D

(Security classification of title, body of abstract and indexing annotation must be entered when the overall report is classified)

1. ORIGINATING ACTIVITY *(Corporate author)* Aerospace Medical Research Laboratories Aerospace Medical Division, Air Force Systems Command, Wright-Patterson AFB, Ohio 45433	2a. REPORT SECURITY CLASSIFICATION UNCLASSIFIED 2b. GROUP N/A

3. REPORT TITLE

EVALUATION OF TWO CYCLIC-STRAIN IMPACT ATTENUATORS

4. DESCRIPTIVE NOTES *(Type of report and inclusive dates)*

5. AUTHOR(S) *(First name, middle initial, last name)*

Managan, Richard F., Chief Master Sergeant
Flagg, Kenneth C., Second Lieutenant, USAF
Clarke, Neville P., Major, USAF, VC
Duddy, John H.

6. REPORT DATE May 1967	7a. TOTAL NO. OF PAGES 16	7b. NO. OF REFS 0
8a. CONTRACT OR GRANT NO. b. PROJECT NO. 6301 c. Task No. 630102 d.	9a. ORIGINATOR'S REPORT NUMBER(S) 9b. OTHER REPORT NO(S) *(Any other numbers that may be assigned this report)* AMRL-TR-66-221	

10. DISTRIBUTION STATEMENT

Distribution of this document is unlimited.

11. SUPPLEMENTARY NOTES	12. SPONSORING MILITARY ACTIVITY Aerospace Medical Research Laboratories Aerospace Medical Div., Air Force Systems Command, Wright-Patterson AFB, O. 45433

13. ABSTRACT

Two impact energy attenuators operating on the principle of cyclic straining of materials were tested to determine: (1) maximum output accelerations and (2) resultant attenuator deflections. The attenuators were tested in tension with initial impact velocities from 914 to 1338 centimeters per second and maximum input accelerations from 21 G to 58 G. The attenuators were tested in compression with initial impact velocities from 546 to 855 centimeters per second. The maximum output acceleration showed dependency upon payload that was consistent with the attenuator design theory.

DD FORM 1 NOV 65 1473

Security Classification

Security Classification

14. KEY WORDS	LINK A		LINK B		LINK C	
	ROLE	WT	ROLE	WT	ROLE	WT
Impact attenuation Personnel protection Landing impact related equipment Attenuation hardware						

Security Classification